Ari J. Tuononen. 2009. On-board estimation of dynamic tyre forces from optically measured tyre carcass deflections. International Journal of Heavy Vehicle Systems, volume 16, number 3, pages 362-378.

On-board estimation of dynamic tyre forces from optically measured tyre carcass deflections

Abstract

Active safety systems would benefit from accurate information on tyre forces. A special sensor module has been developed for research purposes in order to study real-time tyre force estimation from tyre carcass displacements. The forces can be measured in vertical, lateral and longitudinal directions. The sensor measures tyre carcass movement with respect to the rim and transmits the data wirelessly to the chassis. The raw data is analysed and tyre force information is available on a CAN-bus. The sensor is calibrated in a tyre test rig and proving ground measurement results are presented. The lateral and longitudinal force estimates are accurate if compared to the vehicle accelerations, but the vertical force is difficult to estimate during heavy braking manoeuvres.

Keywords:

active safety system; intelligent tyre; optical tyre sensor; tyre deformation; friction estimation; advanced driver assistance, optical position detection

Introduction

Active safety systems have become common equipment in all vehicle categories. Estimation of individual tyre operating states could improve the performance of active safety systems. The tyre transmits all the forces between the chassis and road, and thus dominates the vehicle behaviour. The tyre sensors could offer several different functions:

- tyre pressure monitoring TPMS (the only one in production)
- estimation of tyre forces (vertical, lateral and longitudinal) and aligning moment
- slip ratio and slip angle
- recognition of tyre improper and normal wearing, imbalance
- recognition of worn suspension components

Tyre pressure monitoring is already available and it is extremely beneficial, especially for heavy vehicles as their tyre pressure is sometimes more difficult to check than the pressure of passenger car tyres. The low inflation pressure increases fuel consumption (and CO2), tyre wearing and complicates vehicle behaviour in limit handling. In addition, incorrect inflation pressure changes tyre stiffness and dynamic rolling radius, which may mislead state estimators of active safety systems.

Vertical tyre force estimation is probably the next step after TPMS because it is available from the acceleration sensor attached to the TPMS unit. The acceleration sensor algorithms are discussed, for example in Morinaga (2006). The piezoelectric power source can also be implemented to estimate contact length and contact deformation, which both correlate with vertical force (Mancosu 2007). The first versions of the vertical force tyre sensor may only estimate static vertical force due to load transfer, and not dynamic load. Dynamic wheel load estimation from vehicle sensors is especially difficult in heavy vehicles, due to the influence of the flexible chassis (compared to cars) for roll stiffness distribution. Also, the payload can make load deviation extreme.

The exact vertical force estimate together with existing vehicle sensors provide a good basis for estimating lateral and longitudinal tyre forces, especially for the linear operating range of tyre. Directly measured lateral forces could allow vehicle slip angle estimation in every condition without any tyre parameters like cornering stiffness or friction coefficient.

Detection of broken or worn suspension parts (or tyre) can be difficult to conduct with the use of standard vehicle sensors. In a passenger car the driver can more easily feel if the tyre is badly imbalanced or otherwise damaged than in heavy vehicles. The tyre sensor can detect such a phenomenon, for example by comparing the wheel load deviation of neighbouring wheels. This might also reveal worn damper or other potential problems which are not otherwise easily observed.

This paper introduces an optical tyre sensor for a truck. Even if the optical measurement devices offer some outstanding advantages, the sensor in question is not intended to be a commercial product. Meanwhile, the optical tyre sensor module is being developed in order to serve as a research platform. It offers an opportunity to study which functions could be useful when considering product sensors.

Optical tyre sensor module and test vehicle

The optical tyre sensor was developed in the EC-funded Apollo-project 2002-2005 and has been further developed in the FRICTION project (APOLLO 2005, FRICTION 2006 and Tuononen 2008). The sensor requires some space in the rim, and once the sensor is installed, it is not possible to install or remove the tyre anymore. In passenger car rims this problem was avoided by using dividable rims. On the contrary, a dividable truck rim was not an attractive option because of tedious assembly work and the iterative nature of sensor development. Therefore, a special sensor module was designed to interface the rim (Figure 1). The sensor module can be quickly removed and reinstalled without special tools.

Figure 1 Sensor module installation to the test rim
(1. rim, 2 flange joint welded to the rim, 3. sensor module 5. sealing O-ring)

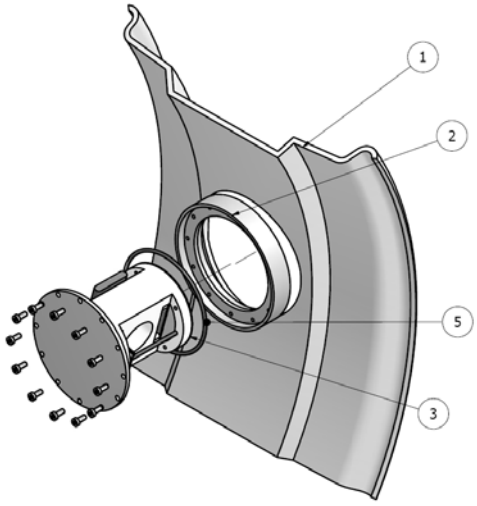

The tyre is installed before the sensor module and the LED (Light Emitting Diode) is glued into the inner liner of the tyre (Figure 3). The LED is powered with wires from the sensor module. In addition to the sensor module, a magnetic pick-up sensor is installed on the inner edge of rim (Figure 4). The magnet is installed on the suspension to indicate the upright position of the sensor. This enables very accurate information on the sensor rotation angle and the data is certainly on the same time axis as the actual tyre sensor data, due to same signal path.

The actual tyre sensor is a light sensitive device called a PSD (Position sensitive detector). The PSD sensor (Hamamatsu S5991-01 Pin cushion) converts the light energy to currents, which are measured from the corners of the sensor. The active area of the sensor is 10mmx10mm, the position resolution is 1.5µm, rise time is 2µs and photo sensitivity is 0.6 A/W [Hamamatsu 2008]. The actual displacements can be calculated:

$$x = \frac{L}{2}\frac{(i_{x2}+i_{y1})-(i_{x1}+i_{y2})}{i_{x2}+i_{y1}+i_{x1}+i_{y2}} \quad (1)$$

$$y = \frac{L}{2}\frac{(i_{x2}+i_{y2})-(i_{x1}+i_{y1})}{i_{x2}+i_{y1}+i_{x1}+i_{y2}} \quad (2)$$

$$z = \sqrt{\frac{1}{i_{x2}+i_{y1}+i_{x1}+i_{y2}}} \quad (3)$$

where i indicates respective current and L is length of the sensor active area. Figure 2 clarifies the PSD structure and how the output current depends on position of light spot on active area of the sensor.

Figure 2 The PSD sensor structure [Hamamatsu 2003]

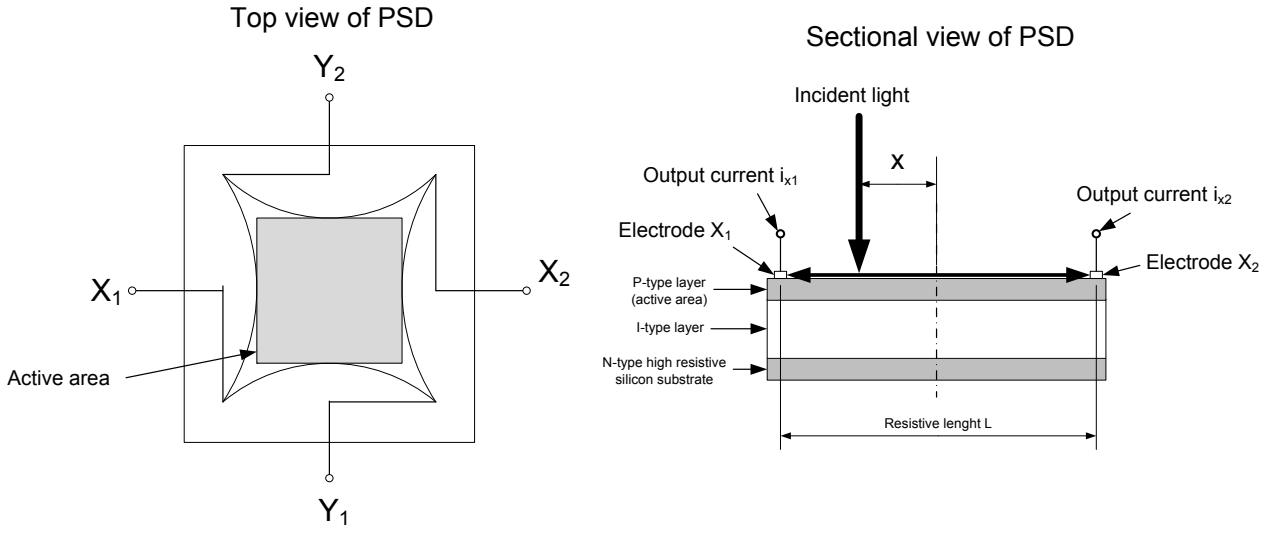

However, the real-time displacement calculation was a bit different: only additions and subtractions were executed for analogue signals. Basically the operational amplifiers calculated equations:

$$V_x = G_x\left[(i_{x2} + i_{y1}) - (i_{x1} + i_{y2})\right] \quad (4)$$

$$V_y = G_y\left[(i_{x2} + i_{y2}) - (i_{x1} + i_{y1})\right] \quad (5)$$

$$V_{sum} = G_{sum}\left[i_{x2} + i_{y1} + i_{x1} + i_{y2}\right] \quad (6)$$

where G_x, G_y and G_{sum} are respective gains. The voltages are amplified and measured with ADC. The MCU prepares the message including Cyclic Redundancy Check (CRC) to be sent by the radio. The radio operates on 433.92Mz. The radio receiver is located next to the tyre (Figure 8). The data is demodulated and converted to the CAN-message for the 1Mbps bus. This displacement data is further analysed in a 16-bit MCU which calculates vertical, longitudinal and lateral tyre forces and sends the data to the 250kbps CAN-

bus. This additional processing step was taken because otherwise tyre sensor raw data (sampled 5100Hz for each channel) loaded the data acquisition to the limits. Figure 5 shows the complete signal path.

The sensor and transmitter are powered by a Li-ion battery adopted from a mobile phone. The battery is charged through a pressure proof connector in the rim. The circularly polarized antenna and receiver unit, which can be seen in Figure 8, are installed close to the tyre.

Figure 3 Cross-section of optical tyre sensor

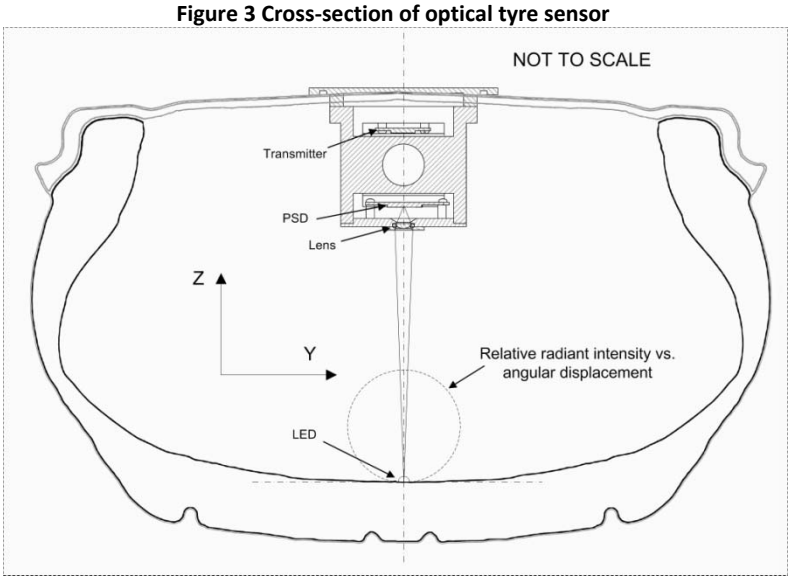

Figure 4 Optical tyre sensor components, magnet and magnetic pick-up sensor

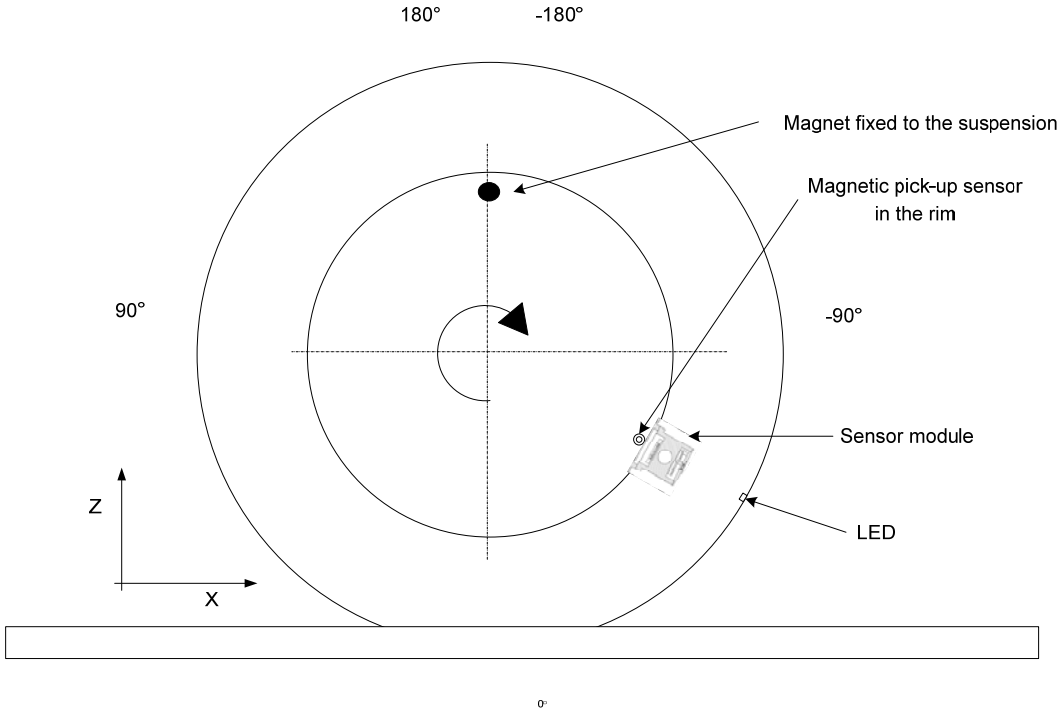

Figure 5 Signal flow from sensor to the data acquisition

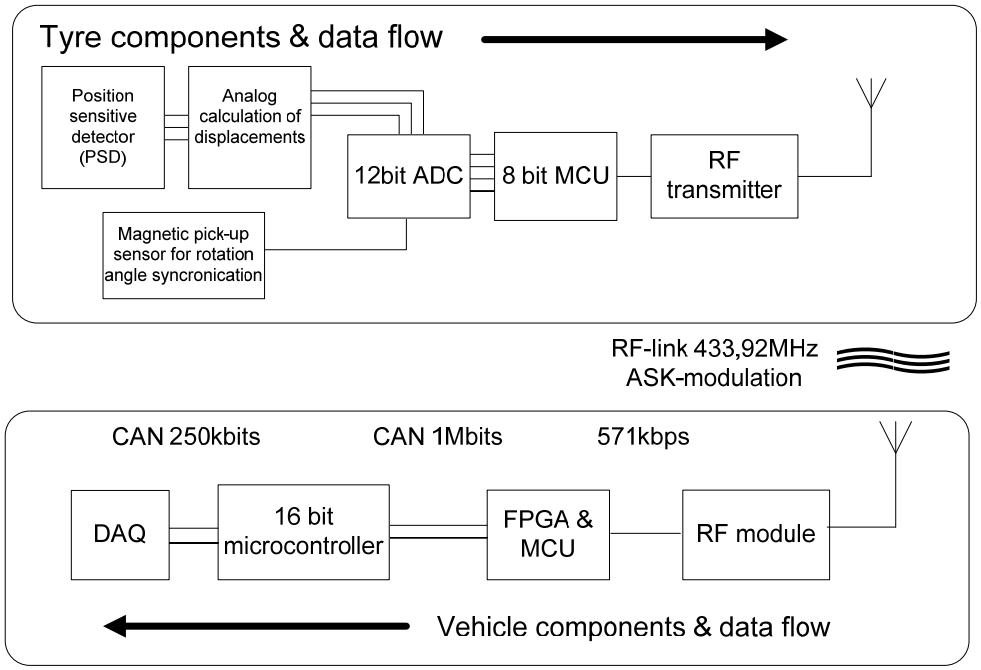

The optical tyre sensor output signals for approximately two rotations are shown in Figure 6. The magnetic pick-up sensor signal is found between the contacts (magnet and sensor position are shown in Figure 4), which are expected from the upright position of the magnet. The intensity signal (W/m^2) shows decreased intensity during contact. The vertical displacement (inverse square relation to intensity) can be calculated:

$$z = \sqrt{\frac{1}{4095 - I_{PSD}}} \tag{7}$$

where the 4095 comes from the inverse configuration of the 12 bit ADC and I_{PSD} is measured intensity. The longitudinal signal shows how the contact deformation constrains the tyre carcass in different directions on the leading and trailing edge. This stress is released only in the exact upright and downright positions of the tyre in free rolling, which can be detected from offset line (dash-line). The lateral signal is not influenced noticeably in free rolling; only slight movement can be detected during contact. This can be explained by tyre force generation from the asymmetry of the tyre or alignment errors of the LED and sensor modules.

Figure 6 Sensor signals in free rolling (50kph, 20kN)

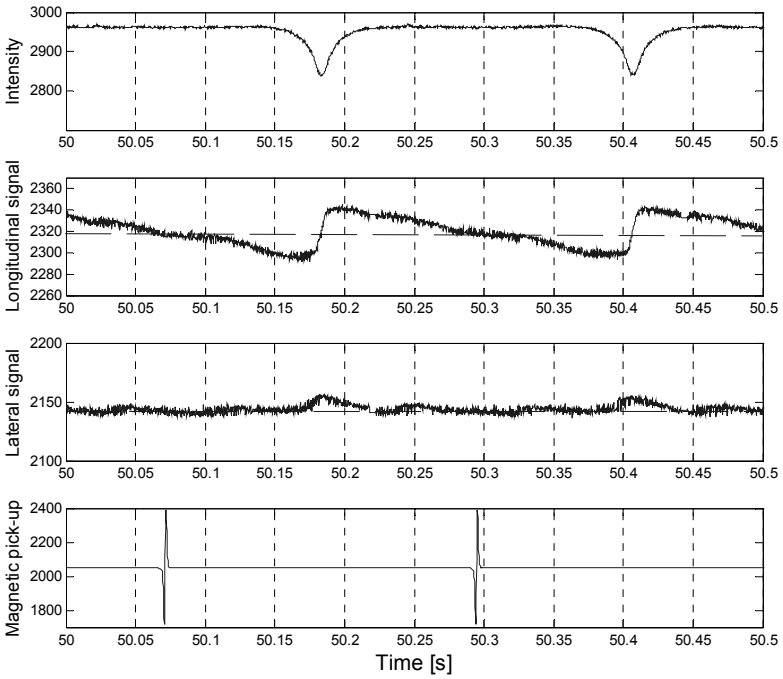

The influence of the slip angle can be seen in Figure 7. The generated lateral force stretches the carcass laterally and the peak value is naturally detected during contact. The increased vertical force, compared to Figure 6, can be seen in intensity and longitudinal signal amplitudes.

Figure 7 Sensor signal under 6° slip angle (50kph, 30kN)

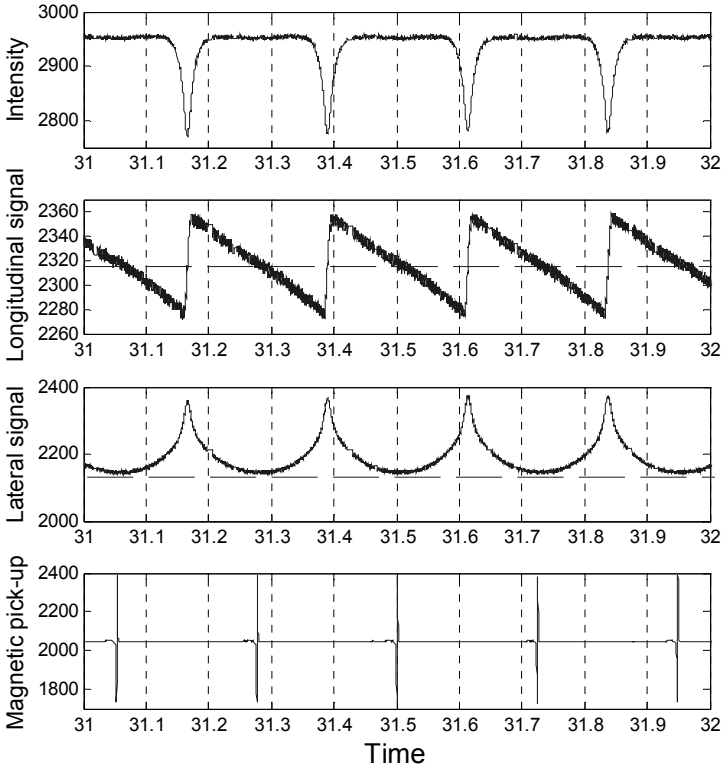

The optical tyre sensor and receiver unit was installed into a Volvo FH12 (Figure 8) tractor with a ballast platform (without trailer). In addition to the tyre sensor and existing ABS/ESC-sensors, the vehicle was equipped with an Inertial Measurement Unit (IMU). The IMU measured 3 degree of freedom accelerations and rotational velocities at 100Hz. The IMU signals were filtered with a transfer function:

$$G(s) = \frac{s^2+65^2}{s^2+65s+65^2} \quad (8)$$

which was discretized with Tustin approximation. The natural frequency for IMU position in the cabin was approximately 65 rad/s, which explains the filter parameters.

Figure 8 Test vehicle Volvo FH12 with tyre sensor receiver unit next to left front wheel

Force estimation algorithms

Tyre force test rig measurements were needed to calibrate force estimation parameters. The tyre test rig at ika RWTH (Institut für Kraftfahrwesen Aachen) satisfied all the requirements for the force levels and for the minimum acceptable radius of the drum. All the calibration measurements were accomplished at the ika RWTH tyre test rig [Holtschulze 2006, Hüsemann 2007].

The tyre force estimate is calculated once per revolution. This means that update frequency depends on the rotational velocity of the wheel (Figure 9). The relationship can be simply expressed:

$$f_{update} = \frac{v}{2\pi\, r_{dyn}} \quad (9)$$

where v is vehicle velocity and r_{dyn} dynamic rolling radius of the tyre. The update rate naturally increases with speed, but on the contrary the number of samples per rotation decreases (Figure 9). The sampling rate for the optical tyre sensor is approximately 5100Hz for each channel, so the number of samples for one revolution reads:

$$N_{samples} = \frac{5100Hz}{v} 2\pi\, r_{dyn} \quad (10)$$

Figure 9 Update frequency and amount of samples per rotation dependence on velocity (r_{dyn} = 0,492m)

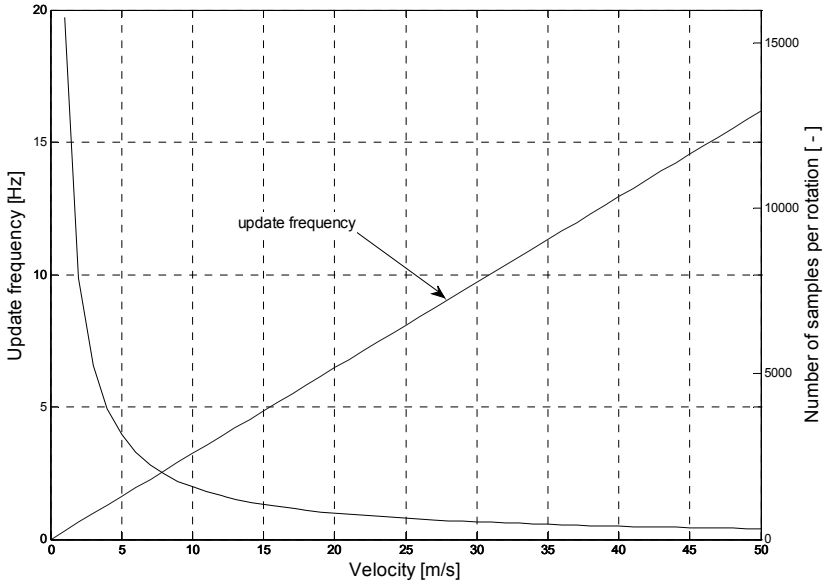

The parameters for upcoming force estimation models are calculated by linear least squares fitting:

$$\bar{c} = (X^T X)^{-1} X^T Y \quad (11)$$

where X is tyre sensor data, Y is test rig data and $\bar{c}$ is set of model parameters.

Vertical force (wheel load)

Vertical force could be estimated from the intensity (eq. 6 and 7) or longitudinal signal (eq. 4). The intensity signal is a natural starting point because it is clear that the contact deformation has to be correlated with the vertical force. However, under lateral force the LED is shifted in a lateral direction and thus the distance between LED and PSD is greater, even if there is no vertical movement at all. This would disturb the vertical force estimation based on intensity signal. Furthermore, LED intensity depends on temperature, LED alignment and supply voltage, but lateral and longitudinal signals are independent of these.

Vertical force has influence on contact length equally. Thus, the contact length could be indicated by the longitudinal signal amplitudes or the peak locations. Also, standard deviation of the longitudinal signal correlates with vertical force. Nevertheless, longitudinal signal amplitude is implemented in this study. The amplitude is calculated:

$$x_{gap} = \max[x_0, x_{end}] - \min[x_0, x_{end}] \quad (12)$$

where [x_0, x_{end}] includes all the x values for one complete rotation.

This is not the best formulation against noise in the signal, but the real time capability has to be fulfilled as well. Furthermore, the signal to noise ratio of the longitudinal signal is quite good for typical wheel loads in trucks. The vertical force estimation reads:

$$F_z = x_{gap}^2 c_{z,parabolic} + x_{gap} c_{z,gain} + c_{z,offset} + \left[\bar{x} c_{z,x\ gain} + c_{z,x\ offset}\right] \quad (13)$$

where the parabolic term is needed due to the inverse square relation of intensity and displacement. The $\bar{x}$, $c_{z,x\ gain}$, and $c_{z,x\ offset}$ terms are needed to compensate the vertical force estimate under longitudinal force, which slightly increases signal amplitude. The calculation of $\bar{x}$ is explained in the longitudinal force estimation section. The vertical force comparison for the test rig measurement is shown in Figure 10.

Figure 10 Tyre sensor and test rig comparison for vertical force

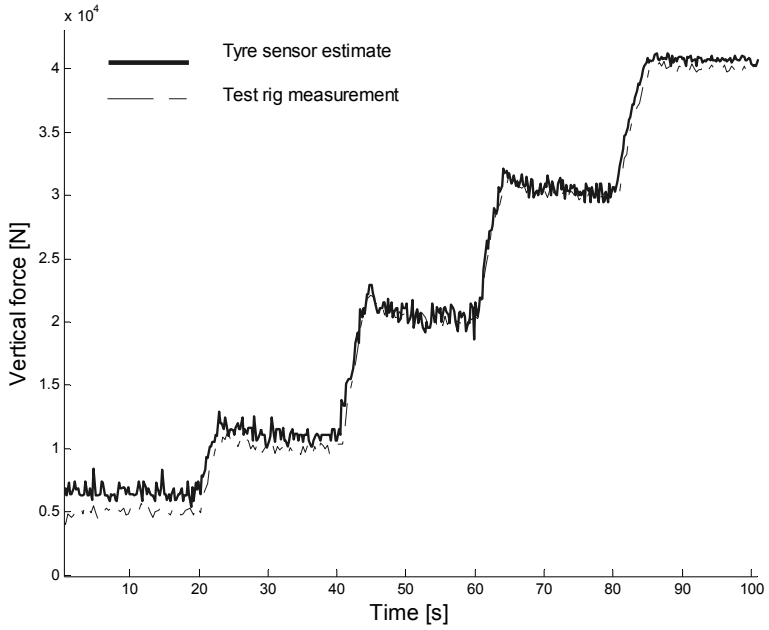

Lateral force

The lateral force can be calculated only from the lateral displacement signal. The peak value of signal correlates with lateral force, but the most robust operation is achieved from the mean value of one rotation. The lateral signal mean value for one rotation can be calculated recursively:

$$\overline{y}_{k+1} = \overline{y}_k + \frac{y_{k+1} - \overline{y}_k}{k} \tag{14}$$

where $\overline{y}_k$ is reset to zero after each rotation. The lateral force reads:

$$F_y = \bar{y}\, c_{y,gain} + c_{y,offset} \tag{15}$$

and the comparisons for test rig measurements are shown in Figure 11.

Figure 11 Lateral force estimate from the tyre sensor compared to the test rig measurements (slip angle sweep +-6°, 50kph, wheel load 10kN 20kN 30kN)

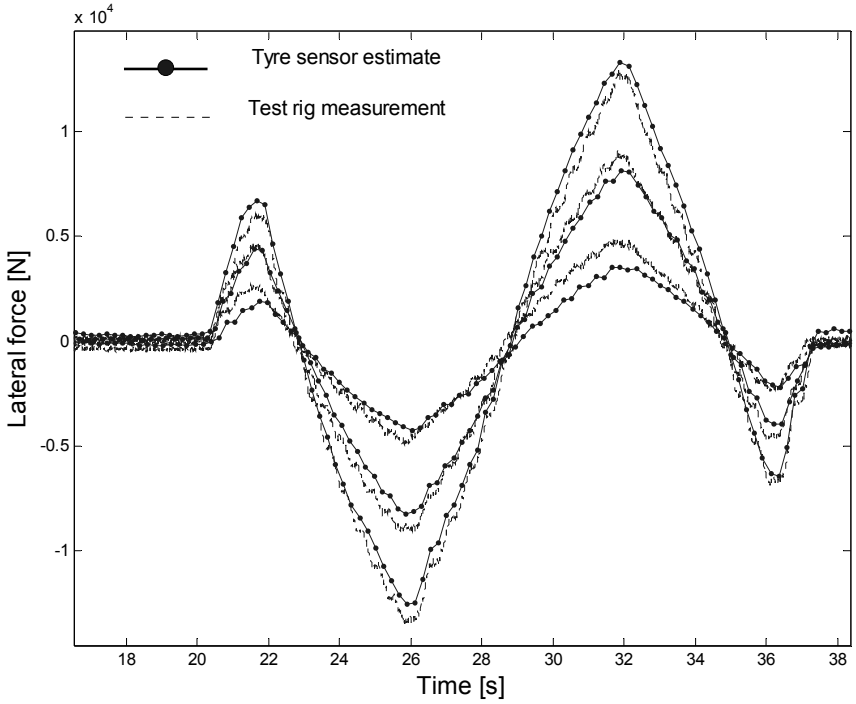

Longitudinal force

The longitudinal signal offers the possibility to estimate longitudinal force. Whereas the amplitude of longitudinal signal indicates the vertical force, the mean value of longitudinal signal can be implemented for longitudinal force estimation. The formula for estimating longitudinal force is adopted from the lateral force estimation, but naturally the longitudinal signal is exploited instead of the lateral one:

$$\overline{x}_{k+1} = \overline{x}_k + \frac{x_{k+1} - \overline{x}_k}{k} \tag{16}$$

The longitudinal force reads:

$$F_x = \bar{x}\, c_{x,gain} + c_{x,offset} \tag{17}$$

and the comparisons for test rig measurements are shown in Figure 12.

Figure 12 Longitudinal force estimate and test rig measurement for brake steps with different wheel loads (30 kph, wheel loads 20kN, 30kN and 40kN)

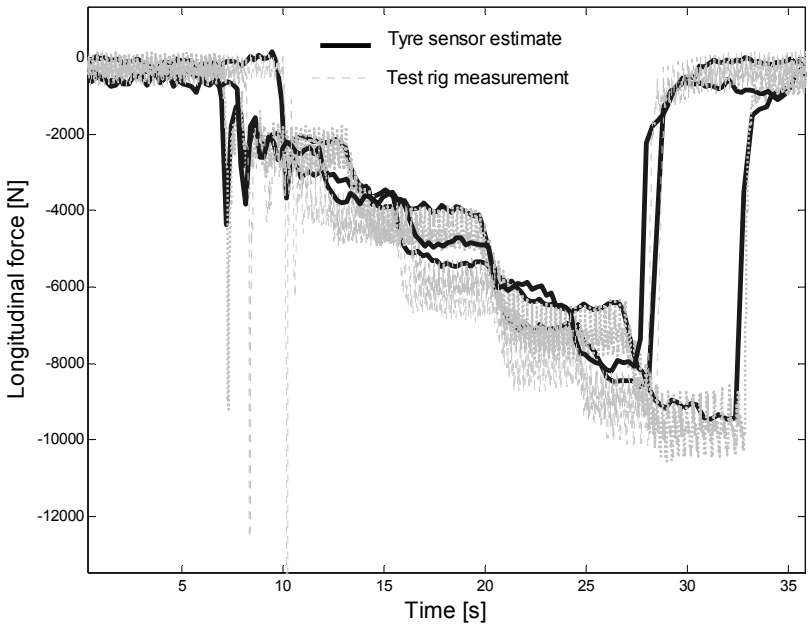

Proving ground vehicle measurements

Steady-state cornering

Constant radius circle measurements were taken by very slowly accelerating the vehicle up to the limit cornering speed. The radius of the circle was 150m. The surface was packed snow on an ice lake. The track was rather bumpy and resulted in great wheel load deviations, which can be observed from the tyre sensor and vehicle acceleration sensor signals.

The normalized lateral force for the tyre sensor (left front tyre) reads:

$$F_{y,n} = \frac{F_y}{F_z} \tag{18}$$

where F_y is the tyre sensor lateral force estimate and F_z is the corresponding vertical force estimate. Lateral acceleration is measured with a standard ESP-sensor. The comparison is shown in Figure 13, where two different measurements are depicted in the same figure (right and left turn). It can be seen that cornering performance is clearly better for the right turn. The tyre sensor estimate matches the acceleration signal quite well, especially for the medium and high accelerations. There is some offset error for the left turn, where the tyre sensor estimate is slightly greater than would be expected from the lateral acceleration. This may come from sensor offsets, or possible toe-out or tyre asymmetry.

A stability control intervention can be observed for the right cornering (loop in 55km/h back to 48 km/h). Figure 14 (same test as that shown in Figure 13) reveals how the tyre sensor is able to measure short brake intervention, which also results in decreased lateral force during braking, following the typical combined slip principle of the tyre.

Figure 13 Lateral acceleration sensor and tyre sensor lateral force estimate for constant radius circle test

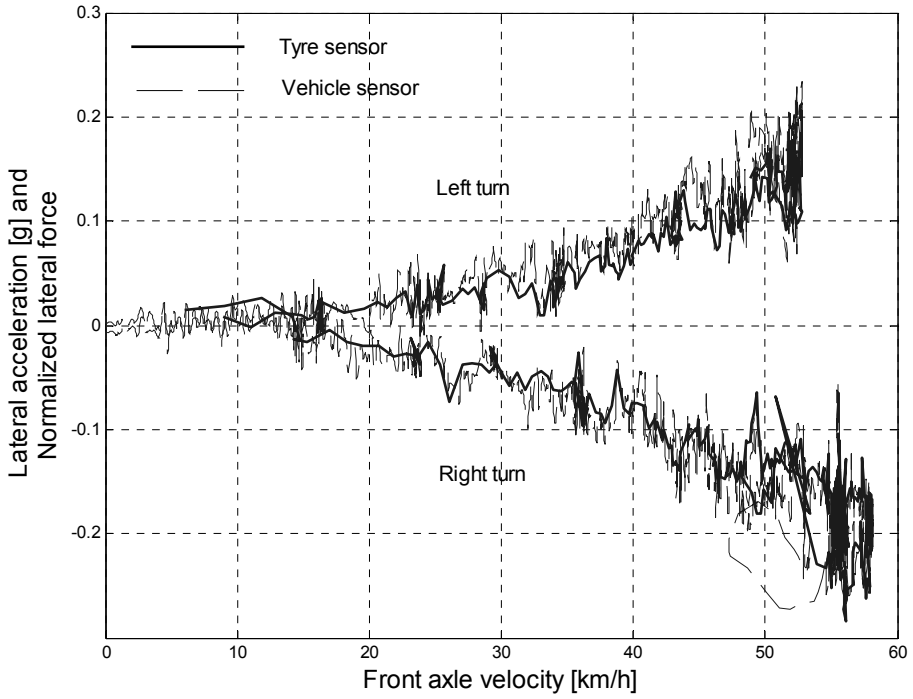

Figure 14 Tyre sensor force estimates during stability control brake intervention for left front wheel

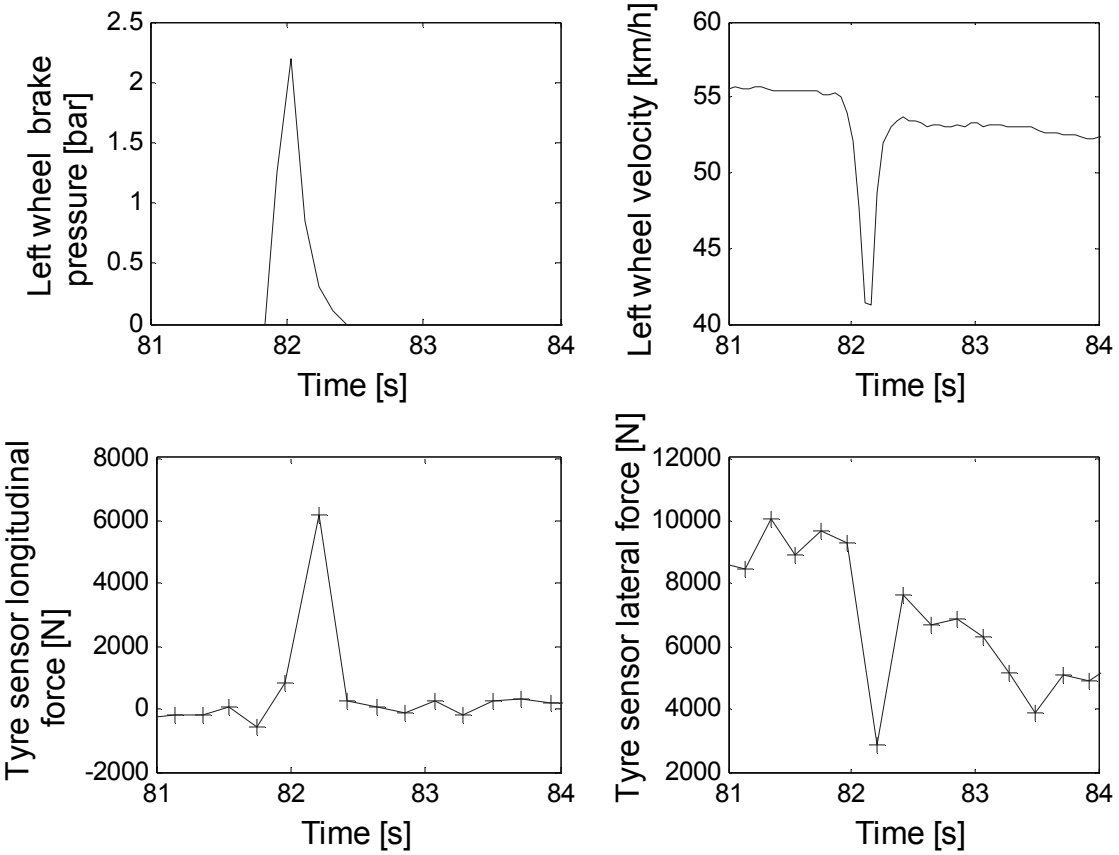

The influence of lateral load transfer in steady state cornering can be seen in Figure 15, where the tyre sensor vertical force is plotted in time domain (same data as for Figure 13). The uneven snow surface results in great wheel load deviations (cf. Figure 10 for even surface vertical force estimate).

Figure 15 Tyre sensor vertical force estimate for constant radius circle test

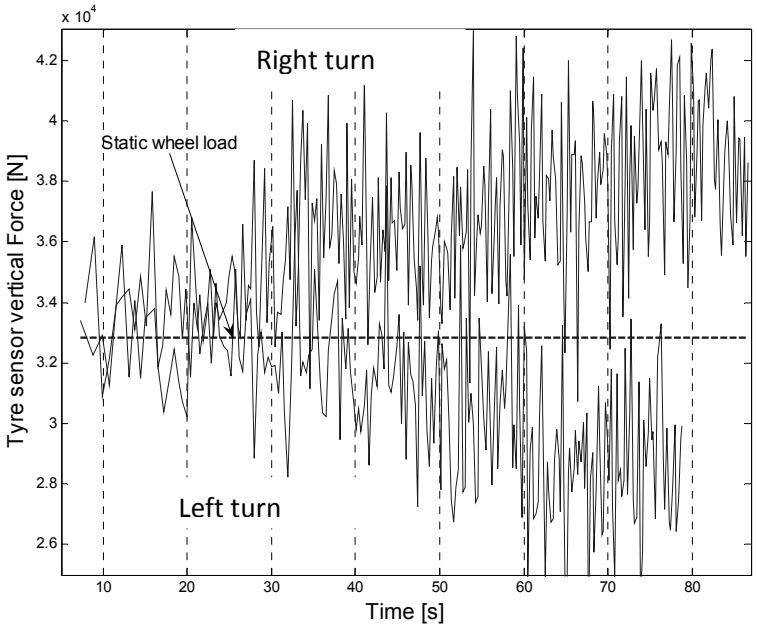

Lane change tests

Figure 16 shows the lateral acceleration measurement and normalized lateral force estimate for sequential lane changes on packed snow. The measurement and estimate match quite well during the left turn (negative values) when the load transfer is away from the sensor tyre.

Figure 16 Lateral acceleration sensor and tyre sensor lateral force estimate for lane changes (packed snow, 55km/h)

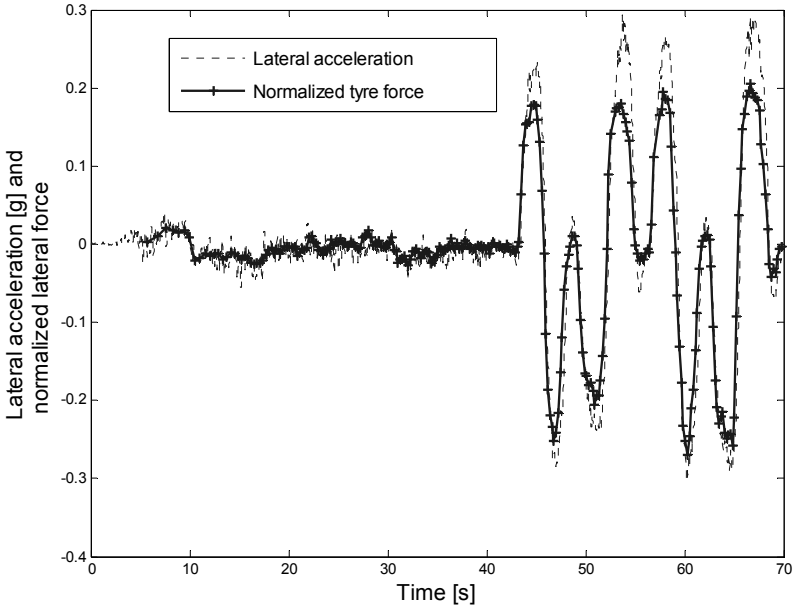

Possible errors for the lateral acceleration signal are:

- Roll angle introduces a gravity component to the measured body lateral acceleration $\dot{v}_y = \frac{a_y - g\sin\theta}{\cos\theta}$ where a_y is the measured acceleration and θ is the roll angle
- Lateral acceleration sensor is not aligned with the tyre sensor, thus in transient manoeuvre yaw acceleration has influence on lateral acceleration at the front axle $a_{y,front} = a_y + r\dot{\omega}$

but neither of these can compensate observed bias between acceleration measurement and tyre force estimate.

Furthermore, it has been observed that tyre sensor overestimates vertical force in some combined slip conditions and this results in underestimation of the normalized lateral force.

However, the data in Figure 16 should not match exactly because measured lateral acceleration describes the lateral force requirement for a complete vehicle, but the normalized tyre force describes the contribution of that particular tyre.

The influence of longitudinal acceleration and lane changes for vertical force can be seen in Figure 17, which is from the same measurement as Figure 16. The longitudinal load transfer during acceleration can be observed from the decreased vertical force. The vertical force varies between 24 000N and 40000N during lane changes.

Figure 17 Tyre sensor vertical force estimate for acceleration and lane changes

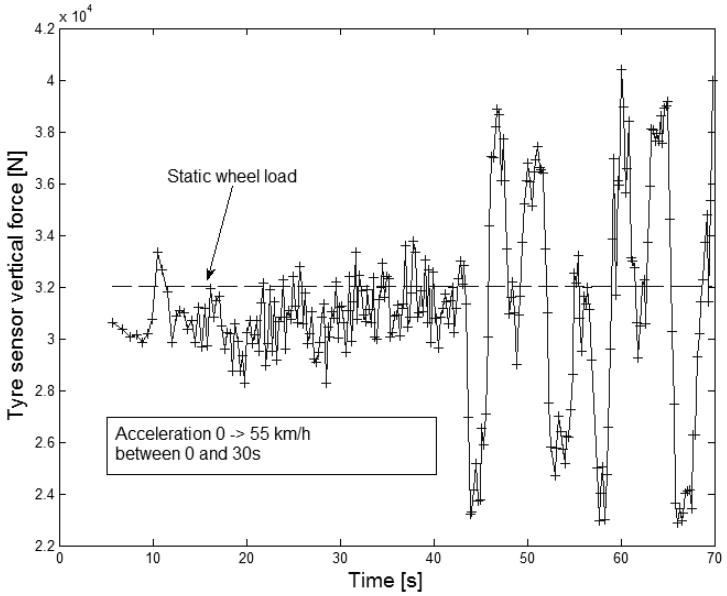

Braking tests

The optical tyre sensor performance to estimate longitudinal force in braking is shown in Figure 19. The brake pressure is increased as a ramp until ABS takes control of the wheel speed after six seconds. The contribution of the left front wheel for the vehicle deceleration is approximated:

$$a_{x,tyre} = g\frac{F_{x,tyre}}{F_{z,tyre}} \quad (19)$$

where vertical force of the left front wheel during deceleration a_x is:

$$F_{z,tyre} = \frac{g\ m\ b + m\ a_x\ h}{2(a+b)} \quad (20)$$

where m is vehicle mass, b is rear axle distance from centre of gravity, a is front axle distance from centre of gravity and h is height of the centre of gravity. Furthermore, pitch introduces some gravity component (Figure 18) for the measured longitudinal acceleration and it is calculated for the global coordinate:

$$a_x = \frac{a_{x,body} - 9.81 \sin(\varphi)}{\cos(\varphi)} \quad (21)$$

where the pitch is simply calculated from the measured pitch rate:

$$\varphi_t = \int_0^t \dot{\varphi} dt \quad (22)$$

which is acceptable for a short period and if the pitch rate sensor offset is exactly known.

Figure 18 Gravity component in measured longitudinal acceleration $a_{x,body}$

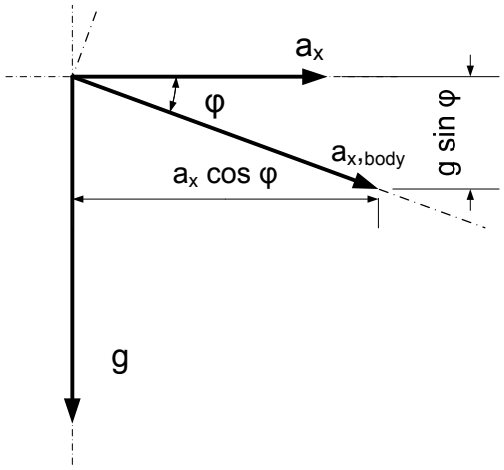

The tyre force estimate is slightly too low when compared to the vehicle sensor (Figure 19). The tyre sensor estimates the contribution of that particular tyre for braking, whereas the vehicle longitudinal acceleration includes the braking forces of every tyre in the vehicle. In other words, in the comparison it is assumed that tyre generates braking force in linear relation to the wheel load which is not necessarily the case. However, the most significant reason for deviation is probably increased tyre pressure (from increased tyre temperature) in repetitive braking manoeuvres on proving ground. This leads to a stiffer tyre and thus the tyre forces are slightly underestimated.

Figure 19 Longitudinal acceleration and tyre sensor estimate for ramp braking

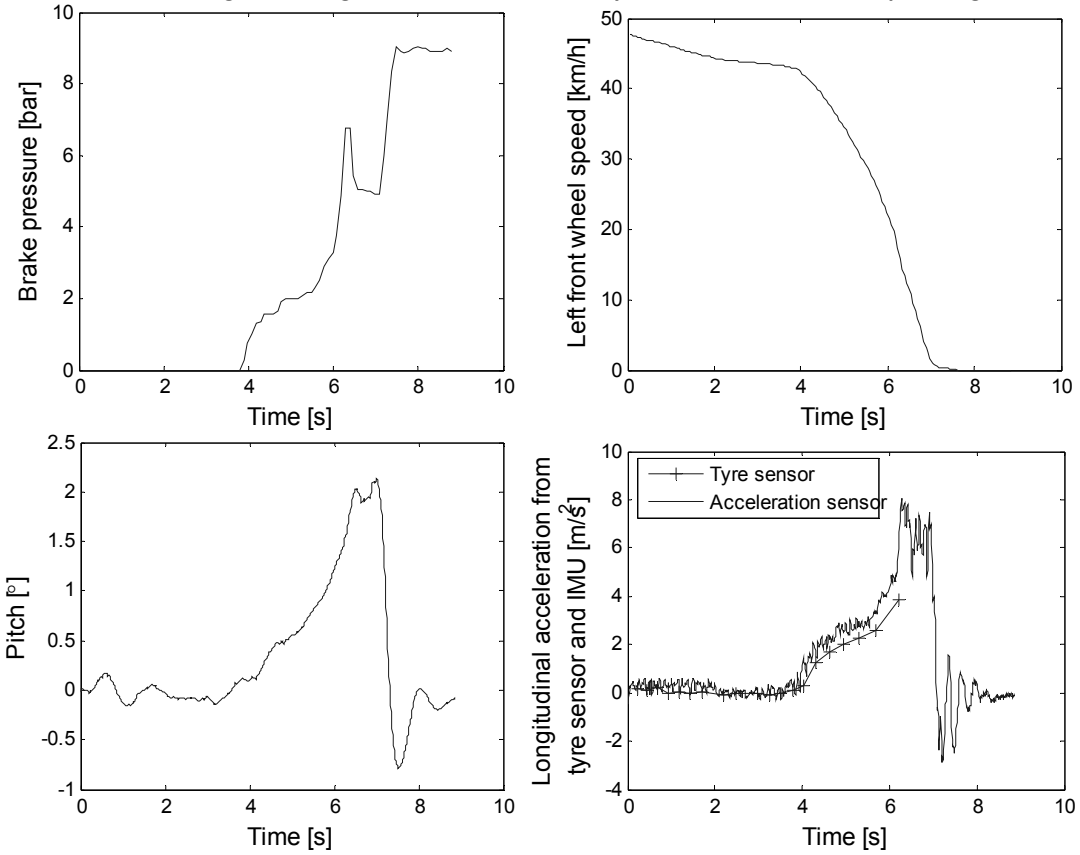

Figure 19 also shows how the tyre sensor cannot update force estimate for low velocities. There is no new tyre force information available after 6.2s (last marker), when the left wheel velocity is approximately 15km/h. The vehicle stopped so quickly after that moment that the new rotation for the tyre sensor was never completed. In addition, possible locking of the wheel at the end of braking would disable tyre force estimation.

Conclusion

The presented optical tyre sensor has proven to be a powerful tool for measuring dynamic tyre carcass displacements. The sensor and the presented algorithms are fully real-time capable in standard low cost MCUs. The lateral and longitudinal force estimates seem to be accurate in most conditions, but the vertical force estimate is not reliable in heavy braking. Even if the tyre force estimates are available only once per revolution, transients such as stability control brake intervention can be captured.

The accuracy of the optical tyre sensor depends mostly on the parameters, which are highly related to the inflation pressure. However, the inflation pressure is varied due to the temperature of the air or nitrogen in the tyre if leakage is neglected. Thus, the measurement of tyre pressure would improve the accuracy of the optical tyre sensor considerably and not complicate the algorithm notably.

Further research could be done with a second tyre sensor on the rear axle of the tractor and a third one on the trailer. This would make it possible to estimate the state of the vehicle very accurately. On the other hand, several tyre sensors on the trailer could be used to study imbalanced tyre detection algorithms.

Acknowledgements

This work was financially supported by EU-project FRICTION FP6-IST-2004-4-027006.
This support is gratefully acknowledged.

References

APOLLO (2005) , Final report, Available online at: www.vtt.fi/apollo 18.6.2008

FRICTION (2006), webpage, http://friction.vtt.fi/ 18.6.2008

Hamamatsu (2008), Hamamatsu PSD S5991-01 data sheet

Hamamatsu (2003), Hamamatsu PSD selection guide, 2003

Holtschulze, Jens (2006), Analyse der Reifenverformungen für eine Identifikation des Reibwerts und weiterer Betriebsgrößen zur Unterstützung von Fahrdynamikregelsystemen, PhD Thesis, ika RWTH Aachen University, April 2006

Hüsemann, Thomas (2007), Tyres in Motion at ika/fka - tyre investigations and research at at ika/fka Aachen", First FTire User Meeting, fka Aachen, 17.-18. July 2007

Mancosu F., Di Pasquale A. (2007), Adding value to the - Next Generation product Inside Tire, Tire Technology Expo 2007, Cologne

Morinaga, Hiroshi; Wakao, Yasumichi; Hanatsuka; Yasushi; Kobayakawa, Akira (2006), The Possibility of the Intelligent Tire (Technology of Contact Area Information Sensing), FISITA 2006, Yokohama

Tuononen, Ari J. (2008), 'Optical position detection to measure tyre carcass deflections', Vehicle System Dynamics, 46:6, 471 — 481